Biomicrofluidics ARTICLE scitation.org/journal/bmf

Micro–nanoparticles magnetic trap: Toward high sensitivity and rapid microfluidic continuous flow enzyme immunoassay

Cite as: Biomicrofluidics 14, 014111 (2020); doi: 10.1063/1.5126027
Submitted: 28 August 2019 · Accepted: 20 January 2020 ·
Published Online: 30 January 2020

Pablo E. Guevara-Pantoja,[1,a)] Margarita Sánchez-Domínguez,[2] and Gabriel A. Caballero-Robledo[1,a)]

AFFILIATIONS

[1]Cinvestav-Monterrey, 66600 Apodaca, Nuevo León, Mexico
[2]Centro de Investigación en Materiales Avanzados, S.C. (CIMAV), Unidad Monterrey, Alianza Norte 202, Parque de Investigación e Innovación Tecnológica, Apodaca 66628, Nuevo León, Mexico

[a)]**Authors to whom correspondence should be addressed:** pguevara@cinvestav.mx and g.a.caballero.robledo@gmail.com

ABSTRACT

In this work, we developed a microfluidic system for immunoassays where we combined the use of magnetic nanoparticles as immunosupport, a microfluidic magnetic trap, and a fluorogenic substrate in continuous flow for detection which, together with the optimization of the functionalization of surfaces to minimize nonspecific interactions, resulted in a detection limit in the order of femtomolar and a total assay time of 40 min for antibiotin antibody detection. A magnetic trap made of carbonyl-iron microparticles packaged inside a 200 μm square microchannel was used to immobilize and concentrate nanoparticles. We functionalized the surface of the iron microparticles with a silica-polyethylene glycol (PEG) shell to avoid corrosion and unspecific protein binding. A new one-step method was developed to coat acrylic microchannels with an organofunctional silane functionalized with PEG to minimize unspecific binding. A model immunoassay was performed using nanoparticles decorated with biotin to capture antibiotin rabbit Immunoglobulin G (IgG) as target primary antibody. The detection was made using antirabbit IgG labeled with the enzyme alkaline phosphatase as a secondary antibody, and we measured fluorescence with a fluorescence microscope. All steps of the immunoassay were performed inside the chip. A calibration curve was obtained in which a detection limit of 8 pg/ml of antibiotin antibody was quantified. The simplicity of the device and the fact that it is made of acrylic, which is compatible with mass production, make it ideal for Point-Of-Care applications.

I. INTRODUCTION

Precise and early diagnosis of a disease can have an immense impact on the degree of success of a treatment. But early diagnosis is typically preceded by the detection of a biomarker present at low concentration in a body fluid sample. Blood chemistry, immunoassays, nucleic acids amplifications, and flow cytometry are the most common techniques that allow for such detection.[1] Nowadays, the degree of sensitivity, specificity, and accuracy of these techniques is extremely good, to the point of being able to detect a single molecule in a sample. However, these techniques usually require long assay times, sophisticated equipment, and a highly trained person to correctly collect the sample, perform the assay, and interpret the results. For these reasons, early and precise diagnosis in developing countries and remote places is more difficult to perform.[2]

Significant efforts have been put in developing Point-Of-Care (POC) diagnostic devices that are cheap, easy to use, and accurate and that do not have the constraints of needing sophisticated laboratories and trained people.[3] The best examples of such devices are the pregnancy and glucose blood level tests. The success of these examples is due in part to the high concentration at which the molecules required for detection are present in the corresponding body fluid. However, if the biomarker of interest is diluted, it becomes equally difficult to create devices with suitable specificity and accuracy.

It is extremely important to produce POC devices capable of performing immunoassays since they are the gold standard analytical tool for protein biomarker detection. Lateral flow systems similar to pregnancy tests have been particularly successful in fulfilling the constraints of POC requirements.[4] Recent developments have managed to improve sensitivity and specificity to excellent

levels for some specific cases.[5] Nevertheless, lateral flow systems have significant limitations including the test results' high dependence on accurate sample input; the need for external peripheral devices to read the output signal for high sensitivity, quantitative tests (fluorescent or optical strip reader); and, more importantly, the difficulty in performing calibration standard curves together with each test in order to provide quantitative results. For these reasons, there is growing interest in developing POC devices based on microfluidics that would allow these limitations to be overcome.[6]

A noncompetitive indirect immunoassay, as those used for allergy diagnosis,[7] requires a series of steps: (1) the incubation of the target–capture antibody–antigen pair, (2) washing of the noncaptured antigens, (3) incubation with detection antibodies, and (4) detection. The use of microfluidic systems to perform immunoassays, together with the use of magnetic micro- and/or nanoparticles as immunosupport, has proven to have enormous advantages with respect to traditional immunoassays: reduction of sample volume, shorter incubation times, automatization of processes, easy and efficient washing, and high detection sensitivity.[8,9]

Micro- or nanoparticles as immunosupport reduce incubation times because the surface-to-volume ratio increases and also because the Brownian movement of the particles improves the kinetics of the reaction between antigen and antibody. Both effects are more pronounced when using nanoparticles compared to the use of microparticles; thus, the protein capture efficiency is maximized with nanoparticles as immunosupport.[10] But at a nanometric scale, the magnetic forces are significantly smaller compared to drag forces due to the high surface–volume ratio. Therefore, trapping the particles with a magnet for subsequent steps (washing and detection) is not efficient. For this reason, Teste *et al.*[11] designed a microfluidic magnetic trap by creating a porous packing of magnetic microparticles through which the solution with the nanoparticles would flow. When an external magnet approaches, strong magnetic field gradients are created between microparticles and, therefore, the magnetic force on the nanoparticles is large enough to capture them and resists flow drag. This system was then used to perform an immunoassay for allergy diagnosis whereby the magnetic nanoparticles grafted with α-lactalbumin acted as Immunoglobulin E capture nanoplataform.[7]

The use of combined magnetic nano- and microparticles allowed Teste *et al.*[7] to have a total assay time of 20 min, which is considerably shorter compared to the hours generally required for a typical assay performed in microtiter plates. However, while achieving a good limit of detection in the order of picomolar (pM), this limit is still high in comparison with standard ELISA tests that can detect analytes in the order of femtomolar (fM), and compared to some microfluidic systems, which can detect analytes on the order of atomolar (aM), it is inferior.[12]

In general, low detection limits can be achieved when fluorogenic enzymatic substrates are used in the detection step: an enzyme is attached to the detection antibody (AbII), which makes the fluorogenic substrate fluorescent. Enzyme-activated fluorogenic substrates are highly sensitive tools because they have an excellent signal-to-noise ratio, much better than conventional chromogenic substrates,[13] since they are measured relative to the absence of light.[14] Table S1 of the supplementary material shows a revision of the literature of microfluidic systems, which detect analytes through immunoassays. The systems are ordered with respect to their detection limit but the table also includes the total assay time. The results indicate that the systems that have the shortest assay times are those that use micro- or nanoparticles as immunosupport, but their detection limits remain relatively high.[7,15–19] In contrast, the systems that use a fluorogenic substrate present low detection limits but longer assay times.[20–26] We attribute the poor sensitivity reported in the literature when using micro- and nanoparticles to the amplification of the nonspecific interactions because of the augmented surface–volume ratio, while long assay times associated with the use of fluorogenic substrates result from the fact that the enzymatic reactions are limited by diffusion.[26]

In this article, we introduce a microfluidic system which combines the use of magnetic nanoparticles as immunosupport, a microfluidic magnetic trap, and a fluorogenic substrate. In addition, we minimized nonspecific interactions by a novel coating of surfaces and by optimizing the packing density of microparticles to maximize the nanoparticles trapping efficiency.[27] All these resulted in immunoassays with a detection limit on the order of fM and a total assay time of 40 min, using biotin as a model antigen and antibiotin rabbit Immunoglobulin G (IgG) as a target analyte.

Our system is fabricated in acrylic, a low-cost thermoplastic that is suitable for the mass production of medical diagnostic devices. This makes our device compatible with mass production processes and, therefore, a good candidate for the development of a POC product.[28]

II. MATERIALS AND METHODS

A. Microfabrication

Microfluidic devices were manufactured on 1.3 mm thick acrylic [polymethylmethacrylate (PMMA)] sheets (ME303018, Goodfellow, USA) by CNC micromilling process (MDX-40A, Roland AG, Germany). The drill bits used to carve out the material were 200 μm and 800 μm square end mill type (Kyocera, 1600-0080L012 and 1600-0320L48), used at a spindle speed of 15 000 rpm and a feed rate of 1 mm/s.

The geometry of the system is shown in Fig. 1(A). The width and depth of the channels are both 200 μm, except in the central area where there are three physical restrictions of only 5 μm depth, which allow the fluid to pass through but retain and amass 7 μm carbonyl-iron microparticles (44 890, Sigma-Aldrich Co., USA) to form three agglomerates of ferromagnetic microparticles. This porous agglomerate acts as magnetic traps for the capture of nanoparticles in the presence of an external magnetic field.[11] We designed the device with three magnetic traps to show the eventual possibility of running several assays in tandem. In the current version, the three magnetic chambers are not independent, but it is clear that they can be easily isolated from each other. Moreover, the design allows us to include as many independent chambers as desired, which would allow a calibration curve to be completed together with each test and obtain quantitative results, similar to what is done in a standard ELISA test. The nanoparticles' capturing efficiency of the traps is not affected by the presence of their neighbors (see Fig. S5 of the supplementary material).

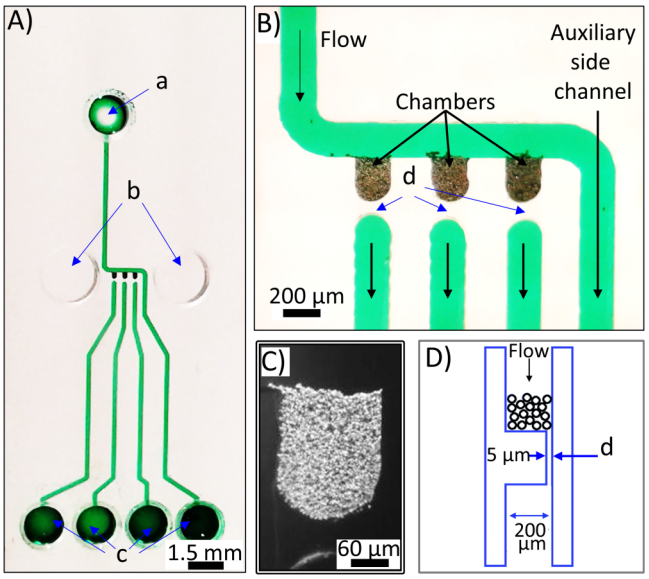

FIG. 1. (A) Microfluidic device filled with green ink: (a) reagents input, (b) cavities into which the poles of the electromagnet enter, and (c) outputs connected to a syringe pump in withdrawal mode. (B) Central zone view of a device with three magnetic traps. (C) Microparticles forming a magnetic trap. (D) Schematic representation of a lateral view of the magnetic trap and physical restriction (d).

The manufacture of the restrictions of 5 μm was particularly difficult because the milling machine has a resolution of 10 μm on vertical displacements. To solve this problem, a piezoelectric actuator was fabricated and coupled to the milling machine, which allowed the manipulation of the vertical axis with high precision.[27–29] The device geometry allows for the introduction of the microparticles through input (a) in Fig. 1(A) to fill the three chambers just above the restrictions (d) shown in Fig. 1(B). Iron microparticles are heavy, which allows for easier handling within the channels so that leftover particles that do not fit within the chambers can easily be removed through the auxiliary side channel by tilting the device. The discarded particles accumulate and remain at the end of the lateral channel, where they do not need to be removed. This protocol allows all the magnetic traps to be made the same size, which is crucial for replication.

In a previous work, we showed that the packing density of the microparticles can be varied by vibrating the microfluidic chip.[27] There, we found that the microparticles trap more nanoparticles when their packing density is small and that the total amount of trapped nanoparticles is of the order of 10^9. When the column of microparticles is formed following the protocol described above, and it is not vibrated, its density is minimal, and the nanoparticle trapping is the most efficient. We characterized the trapping efficiency of the columns of microparticles, and we found that they trap nanoparticles until saturation after a few minutes, depending on the height of the column (see Fig. S3 of the supplementary material).

To seal the channels, a cover of the same material is bonded by pressure, temperature, and solvents, according to a previously reported protocol.[30,28] The device manufacturing and bonding protocol are described in further detail in the supplementary material. Once the acrylic layers are bonded, the pairing and the external tubing (Tygon, ND-100-80, ID 0.02 in., OD 0.06 in.) are glued to their corresponding inlets using regular glue (Resistol 911, Henkel).

A syringe needle, together with its connecting hub, is inserted into the input (a) as shown in Fig. 1(A). The connecting hub functions as a reservoir that can easily be filled with the input reagents using a micropipette. Four glass syringes of 100 μl (Hamilton 1710RNR) mounted on a syringe pump in withdraw mode (Kdscientific KDS-230) are connected to the outputs (c) as shown in Fig. 1(A). A horseshoe shaped electromagnet with direct current power supply was designed and created to generate a 100 mT magnetic field in the area of the magnetic trap. The electromagnet needs to be water-cooled (using a flow rate of 2 ml/s at a temperature of 25 °C) as the electric current needed to generate the desired magnetic field is considerably high (2 A). We used an electromagnet because, in theory, our magnetic trap is capable of capturing and releasing nanoparticles.[27] However, in the case of this application, the releasing of nanoparticles is not needed and, therefore, the electromagnet can be replaced by a simple magnet.

Two cavities [(b) in Fig. 1(A)] were carved onto the acrylic devices in order to insert the electromagnet poles and keep a controlled and fixed position of the electromagnet with respect to the microparticles. The device was mounted on a fluorescence microscope (Axio vert A1, Carl Zeiss Microscopy GmbH, Germany) equipped with a monochromatic camera (IDS, UI-5220SE).

B. Preparation of silica-polyethylene glycol (PEG) coated carbonyl-iron microparticles

Silica and silica-PEG layers were grown on the 7 μm carbonyl-iron microparticles surface to avoid corrosion and unspecific binding of proteins and nanoparticles. The PEG functionalized surfaces are well known to have resistance to protein adsorption, and this property is maximized by covalently binding the PEG to the surface.[31] The microparticles were functionalized by adapting and optimizing a protocol described for iron oxide nanoparticles.[32] No protocol was found in which carbonyl-iron microparticles are functionalized with PEG. The method was based on the Stöber process, in which a silica layer is formed *in situ* by the hydrolysis and condensation of the tetraethyl orthosilicate (TEOS) precursor.[33] Briefly, 1 g of bare carbonyl-iron microparticles (44 890, Sigma-Aldrich Co., USA) was dispersed in 5 ml of ethanol (459 844, Sigma-Aldrich Co., USA), 250 μl of ammonia (320 145, Sigma-Aldrich Co., USA), and 1 ml of TEOS (86 578, Sigma-Aldrich Co., USA). The mixture was stirred for 2 h, avoiding any magnetic mix method. After microparticle precipitation for 5 min, the supernatant was removed and the volume was recovered with clean ethanol; this step was repeated three times. Then, 250 μl of ammonia and 500 μl PEG-APTES (SIM6492, Gelest Inc., USA) were mixed for 1.5 h followed by the addition of 500 μl of TEOS, and a final mixing process of 12 h. Finally, three rinses with ethanol and nitrogen drying were carried out.

C. Acrylic channels functionalization

To avoid nonspecific adsorption of nanoparticles and proteins to the microchannels walls, a chemical treatment was necessary. This treatment was applied to the surface with a silane molecule functionalized with polyethylene glycol (Si-PEG) (SIM6492.7, Gelest Inc., USA).

Modifying the surface of polymers, such as thermoplastics, is an effective way to improve biocompatibility and hydrophilicity while still maintaining its general properties. Several modifications for acrylic have been developed using different techniques such as chemical modification or physical adsorption of molecules and proteins, among others.[34–36] Organofunctional silanes are silane molecules functionalized with a wide variety of molecules and compounds[37] and have been used successfully to functionalize acrylic with amino functional groups.[38] We found in the literature the use of an organofunctional silane functionalized with PEG to coat nanoparticles,[11] and we decided to test it to functionalize acrylic surfaces. As a result, a new one-step method was developed to coat and functionalize the surfaces of the acrylic microchannels with Si-PEG, giving them hydrophilic properties and low adsorption of proteins and nanoparticles. There are protocols described to functionalize acrylic with PEG, but all are laborious and none is applied in a single step.[39,40]

The treatment was applied as follows: A 10% v/v solution of Si-PEG diluted with de-ionized water was prepared. Then, the microchannels were filled with the solution and incubated for 5 min. Finally, the channels were washed three times with 1 ml of de-ionized water flow.

D. Characterization

Carbonyl-iron microparticle surface morphology was examined by scanning electron microscopy (SEM) (JEOL 6010 Plus) with an acceleration voltage of 20 kV and 10 mm of working distance. Coating with a conductive layer was not required. Particle size distribution was analyzed by laser diffraction (Master Sizer 2000, Malvern), using water as a dispersing medium (see Fig. 3). Surface composition analysis was characterized by an X-ray Photoelectron Spectroscopy (XPS) (Escalab 250Xi) using Avantage^{TM} data analysis software. Resistance to thermal oxidation was measured by thermal gravimetric analysis (TGA, SDT Q600 TA Instruments) under a mix of nitrogen and oxygen atmosphere with a heating rate of 10 °C/min.

There are several kinds of nonspecific interactions in our system: nanoparticles–acrylic channels, nanoparticles–microparticles, proteins–acrylic channels, and proteins–microparticles. The best way to test the efficacy of the functionalizations performed on channels and microparticles to reduce nonspecific interactions described above is to perform the immunoassay with and without surface coatings, which we did in Sec. II E. But in addition to this, we performed additional tests where we used similar fluorescent nanoparticles and antibodies to those used for the immunoassay, but being fluorescent, the tests were easier to perform. The two kinds of nanoparticles used in this work were supplied by Ocean Nano Tech, and they were both of the same material and functionalized with oleic acid. Therefore, we expect their interactions with the system's surfaces to be very similar.

Nonspecific adsorption tests on acrylic channels were made to evaluate surface functionalization performance by incubating anti-rabbit IgG labeled with B-rhodamine (Rockland Ab 611-1003) in one case and 10 nm fluorescent nanoparticles (Ocean Nano Tech IRB-10, USA) in the other case for 10 min inside treated and non-treated microchannels. Fluorescence was then measured after washing for 10 min at a flow rate of 100 μl/h with PBS buffer.

For a surface analysis of the microparticles, 1 mg of microparticles were incubated in a tube for 30 min with 100 μl of a solution of 10 nm fluorescent nanoparticles (Ocean Nano Tech IRB-10, USA) at a concentration of 10 NP/μm^3. After three times of washing with PBS buffer, fluorescence due to the remaining adsorbed nanoparticles was measured with fluorescence microscopy. The efficacy of the microparticles coating to reduce nonspecific interactions with antibodies was tested differently and is described in Sec II E.

E. Immunoassays

A model noncompetitive indirect immunoassay was performed by enzyme-labeled antibodies detection. Biotin bound to magnetic nanoparticles (MNPs) of 30 nm (Ocean Nano Tech SHB-30, USA) was used as an antigen (Ag). Our model target primary antibody (AbI) was antibiotin rabbit IgG (Rockland Ab 100-4198) and, as detection or secondary antibody (AbII), antirabbit IgG labeled with the enzyme alkaline phosphatase was used (Rockland Ab 611-1502) together with the fluorogenic enzyme substrate Fluorescein Diphosphate, Tetraammonium Salt (FDP) (Biotium 10030, USA). For these experiments, devices such as those in Fig. 1(A) were used. A syringe needle and its connecting hub connected to the input (a) of Fig. 1(A) acted as a reservoir where the reagents were placed and exchanged as required.

Figure 2(a) shows a graphic representation of the assay protocol: (1) 200 μl of nanoparticles with biotin at a concentration of 0.1 NP/μm^3 is incubated in a tube for 15 min at 35 °C together with 200 μl of the primary antibody at different concentrations (0, 25, 50, 75, 100 pg/ml), using TBS-Tween 20 buffer (0.1% v/v, PH 7.4) as a dilution solution. During incubation, the nanoparticles capture the primary antibody on their antigen decorated surface forming NP–Ag–AbI complexes [Fig. 2(b)]. (2) The solution previously incubated in step one flows through the magnetic trap for 10 min at a flow rate of 100 μl/h, time necessary for the magnetic trap to become saturated with nanoparticles with the primary antibody bonded to them [Fig. 2(c)]. During the whole experiment an external magnetic field is applied to the trap to magnetize it, and it is this magnetic force which bounds the nanoparticles to the microparticles. Trapped nanoparticles remain bounded to the microparticles as long as the external magnetic field is applied, but when it is turned off, the nanoparticles are liberated in a very reproducible manner (see Fig. S5 of the supplementary material). (3) TBS-Tween 20 solution is flown at 100 μl/h for 1 min to wash the non-bonded AbI [Fig. 2(d)]. (4) Detection antibody is injected for 5 min at 20 μl/h at a concentration of 20 μg/ml [Fig. 2(e)]. (5) The nonbonded detection antibody is then washed with TBS-Tween 20 solution for 5 min at a flow rate of 20 μl/h [Fig. 2(f)]. (6) The FDP substrate is injected for 3 min at 20 μl/h [Fig. 2(g)]. (7) Finally, the flow rate of the FDP substrate is adjusted to a specific measurement value (0.5, 1, 2, 5, 10, 20 μl/h) and fluorescence images are taken

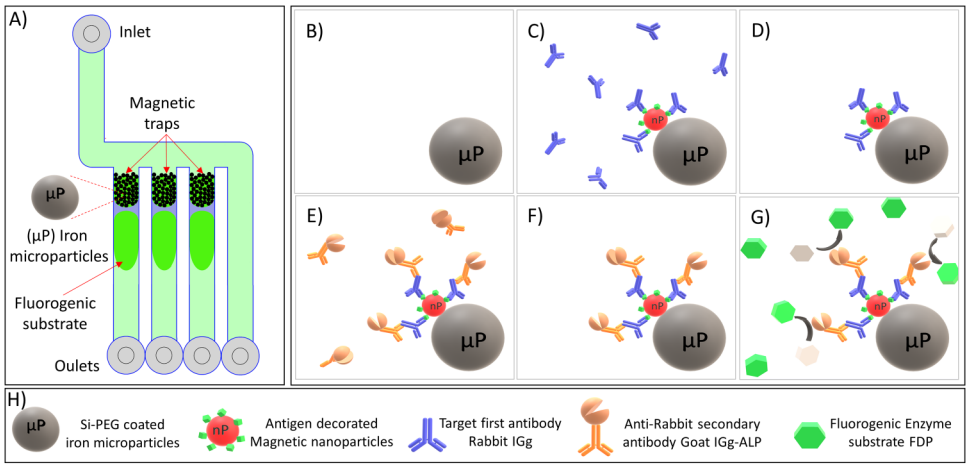

FIG. 2. (a) Schematic representation of the device converting the fluorogenic substrate to its fluorescent state. Graphic representation of immunoassay steps: (b) Microparticle representing magnetic trap at the beginning of the experiment. (c) Flow of nanoparticles-sample mixture through the magnetic trap. (d) Captured nanoparticles after washing the nonbonded primary antibodies. The nanoparticles bound to the microparticles due to the external magnetic field applied to the trap. (e) Incubation with the secondary antibody. (f) Magnetic trap after washing the nonbonded secondary antibodies. (g) The FDP substrate being converted to its fluorescent state. During the whole assay the solutions are flowing through the porous trap and a magnetic field is applied.

with a fluorescence microscope (Axio vert A1, Carl Zeiss Microscopy GmbH, Germany) equipped with a monochromatic camera (IDS, UI-5220SE) which captures the total fluorescence intensity as levels of gray. Using ImageJ (software for image processing in Java), the difference in average fluorescence intensity between the areas near the entrance and near the outlet of the magnetic trap is calculated, which is related to the amount of enzyme trapped in the chamber. The fluorescence of the chip is subtracted to all data. The total time of the assay is approximately 40 min. Signal-to-noise ratio and nonspecific interactions were tested by comparing the complete immunoassay at a flow rate of 5 μl/h and at a AbI concentration of 50 pg/ml to the immunoassay performed without applying the magnetic field, without adding AbI, without adding AbII, and, finally, the efficacy of the microparticles coating was tested by performing the immunoassay without AbI and with noncoated microparticles.

III. RESULTS AND DISCUSSIONS

A. Microparticles characterization

Figure 3(a) shows SEM microscopy images of bare microparticles. Although the particles are spherical, many are composed of several fused spheres of different sizes, which makes them effectively nonspherical. The analysis of the particle size distribution by laser diffraction (Master Sizer 2000) in Fig. 3(b) shows the polydispersity of the microparticles. Using this method, no significant

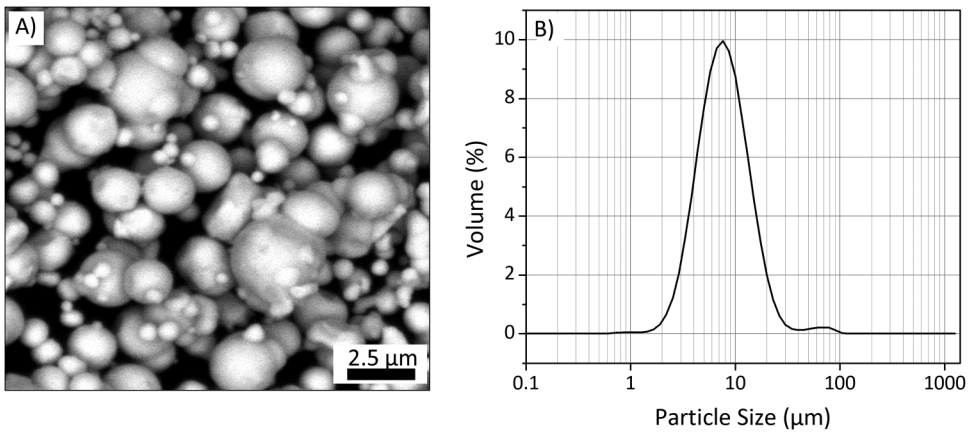

FIG. 3. (a) SEM image of the noncoated iron microparticles. (b) Particle size distribution using laser diffraction.

TABLE I. XPS analysis.

Element	Uncoated (%)	Coated (%)
Si	2.23	22.92
C	30.21	29.04
O	47.43	48.04
Fe	20.13	0
Total	100	100

difference was found between the size of the bare and coated microparticles (see Fig. S6 of the supplementary material).

XPS measurements were made to analyze the elemental composition of the surfaces. Table I shows the results of the analysis of the microparticles with and without the silica-PEG coating. Uncoated particles have a high content of iron (Fe), oxygen (O), carbon (C), and a small amount of silicon (Si). The presence of oxygen is expected from a layer of iron oxide surrounding the microparticles, and carbon is part of the preparation of the sample. In contrast, particles coated with silica-PEG demonstrate a high concentration of silicon (Si) due to the silica-PEG coating though iron (Fe) is absent. This absence indicates that the functionalization of the surface is homogeneous and does not have any coating free areas. The amount of detected oxygen (O) and carbon (C) is very similar in both samples. This technique cannot detect hydrogen. See the supplementary material for the full XPS spectra of both types of microparticles.

Figure 4 shows the results of the thermogravimetric analysis where weight gain is observed as a function of temperature. The weight gain is a result of the oxidation of iron: the iron powder can absorb up to 40% of its mass in oxygen by forming various kinds of iron oxide.[41] A clear difference in resistance to thermal oxidation is observed between functionalized (solid black line) and bare (black dotted line) microparticles: uncoated microparticles begin to oxidize at 200 °C, while coated microparticles begin at 300 °C. This difference is due to the thermo-oxidative protection of the silica layer present on the surface of the microparticles, which delays the oxidation process at a higher temperature. The red curves show the derivative of the weight loss with respect to the temperature of the bare (dotted line) and coated (solid line) microparticles, in which the change of slopes and the difference of oxidation threshold temperatures are more clearly seen. For the covered particles, a peak close to 100 °C is observed, corresponding to the evaporation (loss) of water absorbed in the silica and PEG layer. These results corroborate the XPS analysis which shows that the entire surface of the microparticles is covered by the coating, making them resistant to oxidation.

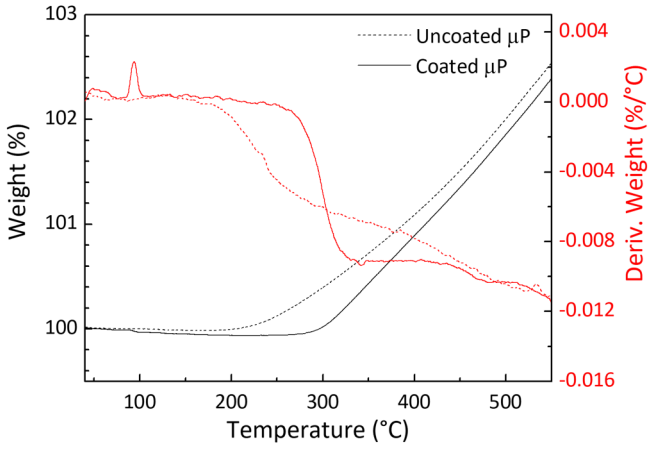

FIG. 4. Thermogravimetric analysis curves of the bare microparticles (dotted lines) and coated with silica and PEG (solid lines). In black, the gain of weight due to the oxidation of iron, and in red, the derivative of weight loss with respect to temperature.

B. Nonspecific interactions of channels and microparticles

Figure 5(a) shows the results of experiments made to test the efficacy of the Si-PEG coatings of acrylic channels to avoid nonspecific interactions with the fluorescent version of the detection antibody (the enzyme is replaced by rhodamine). A solution was flowed with the fluorescent antibody in each channel, without a magnetic trap on them and without an external magnetic field applied, and the remaining fluorescence was measured after washing. Left column [Fig. 5(a)] represents the resulting fluorescence due to adsorbed antibody to the surface of a channel without any treatment. The middle column shows the fluorescence with the adsorbed antibody, but in a channel functionalized with Si-PEG. The fluorescence resulting from the channel treated with Si-PEG is almost the same as the basal fluorescence of a channel that was not in contact with fluorescent antibody. In contrast, in the untreated channel, strong fluorescence is observed from adsorbed antibody that was anchored to the walls of the channel in a nonspecific manner. Experiments with fluorescent nanoparticles were also performed instead of antibody and the same results were obtained (see Fig. S4 of the supplementary material).

We also performed nonspecific adsorption tests between fluorescent nanoparticles and microparticles (without magnetic field). Figure S4B of the supplementary material shows that bare microparticles retain their fluorescence due to the adsorption of nanoparticles, even after washing, while microparticles with the silica layer retain fewer nanoparticles by comparison. However, the best behavior was obtained with the microparticles with the additional layer of silica-PEG where it is observed that the fluorescence falls drastically.

Figure 5(b) shows a complete immunoassay (column 4) compared to immunoassays done under different conditions as controls. It can be seen that most of the noise in our immunoassay comes from the nonspecific interactions of the detection antibody AbII. In addition, if the microparticles are not coated, the nonspecific adsorption of the detection antibody is so strong that the resulting fluorescent signal is saturated, which shows the efficacy and importance of the microparticles coating implemented here.

In conclusion, acrylic channels and microparticles functionalizations are both very effective in avoiding nonspecific interactions

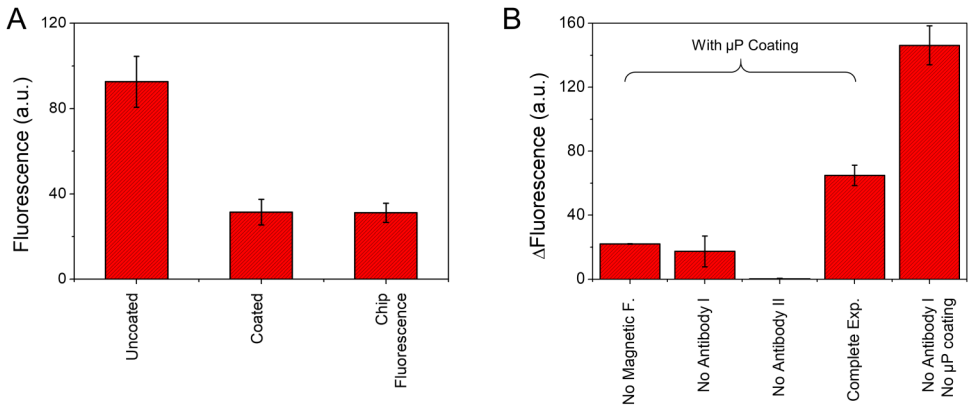

FIG. 5. (a) Channels coating: remnant fluorescence due to nonspecific binding of AbII conjugated with rhodamine at a concentration of 100 μg/ml in uncoated and coated microchannels with silane-PEG. (b) Fluorescence obtained from the complete immunoassay at a flow rate of 5 μl/h and at a AbI concentration of 50 pg/ml is compared to the fluorescence obtained from the immunoassay performed without applying the magnetic field (column 1), without adding AbI (column 2), without adding AbII (column 3), and, finally, the efficacy of the microparticles coating was tested by performing the immunoassay without AbI and with noncoated microparticles (column 5). The level of fluorescence of the two first columns in b results from nonspecific interactions of AbII with the microparticles. Error bars are standard deviation.

with proteins and nanoparticles. This is an essential characteristic in performing immunoassays with high sensitivity, and which is usually the inhibiting factor for the detection limit of microfluidic systems.

C. Proof-of-concept: Immunoassays with a model antibody

Figure 6 shows representative images of the immunoassay experiments at the detection stage, where the complexes Ag–AbI–AbII are attached to the nanoparticles trapped in the magnetic traps and the fluorogenic substrate is flowed at different rates. For the analysis, the difference in average intensity between the areas near the entrance and near the outlet of the magnetic trap is calculated. The measurement areas are indicated in Fig. 6(a) for one of the traps. The average level of gray is calculated for each of the regions of interest using standard image analysis. At lower flow rates, the substrate remains longer inside the trap, increasing its probability of being converted to its fluorescent compound and, therefore, increasing the fluorescent intensity of the signal. The difference of fluorescence intensity at different flow rates can be clearly observed in Figs. 6(b)–6(d).

Figure 7 shows the fluorescence difference from immunoassays at various concentrations of the primary antibody. Each trace corresponds to measurements at a different flow rate of the enzyme substrate. From these results, the limit of detection can be calculated to be 10, 33, 23, and 8 pg/ml corresponding to the flow rates 1, 5, 10, and 20 μl/h. Therefore, our best limit of detection of antibiotin antibody is 8 pg/ml, while the average limit of detection is about 20 pg/ml. The limit of detection is the smallest amount of an analyte, in this case antibodies, whose signal can be distinguished from a blank. It can be calculated as three times the standard deviation of the zero concentration of AbI (the blank) divided by the slope of the calibration curve.[42,10] If the mean of the distributions of measurements of a blank and the mean of the distribution of measurements of an analyte at the limit of detection are separated by three standard deviation units, then there is only a 7% of probability that a measurement can be wrongly classified.[42] The level of fluorescence measured for the zero concentration of AbI comes from nonspecific interactions of the AbII with the microparticles [see Fig. 5(b)]. The large variation of the calculated limit of detection in our experiments comes from the small statistics from which

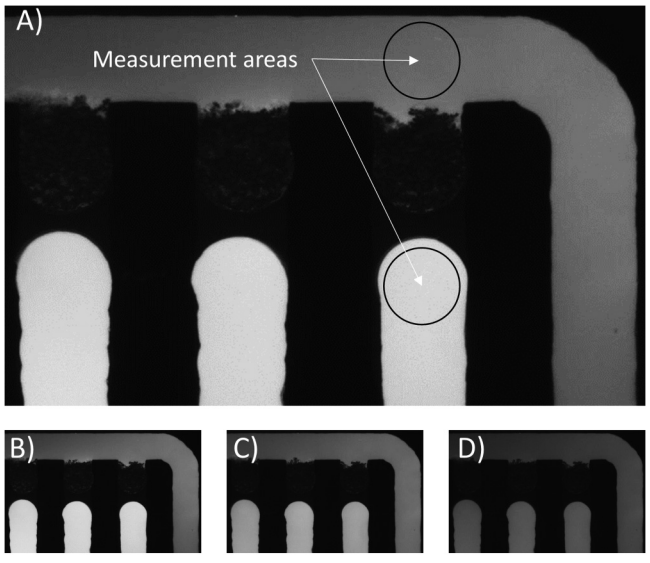

FIG. 6. (a) Typical experiment image in which the measurement areas selected for the fluorescence analysis are shown. Measurement with a flow rate of (a) 1 μl/h, (b) 2 μl/h, (c) 5 μl/h, and (d) 10 μl/h. Experiment at an AbI concentration of 100 pg/ml.

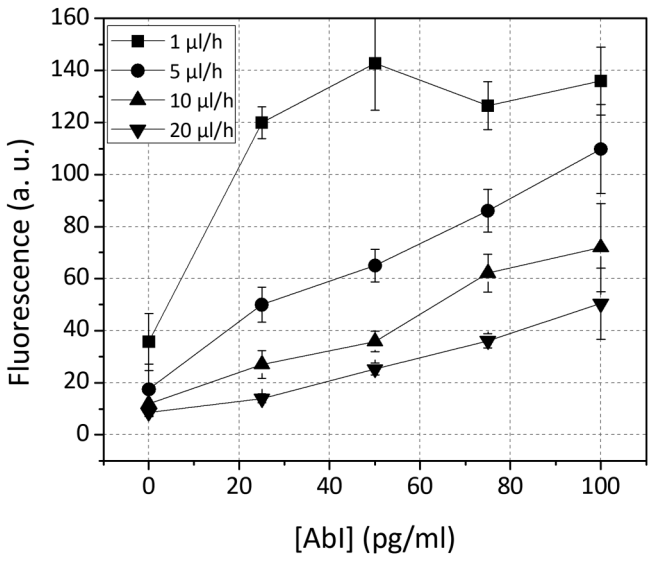

FIG. 7. Calibration curve: fluorescence difference from immunoassays with varying concentrations of AbI at different flow rates of the fluorogenic enzyme substrate. Each experiment was repeated on three different devices.

we determined our blank (only three measurements in each case). Given the large uncertainty on the determination of the blank, we cannot establish the relation between the limit of detection and flow rate. However, the fact that the standard deviation and the slope of the calibration curve are both smaller for larger flow rates suggests that probably the limit of detection is independent of the flow rate.

Using the enzymatic substrate in continuous flow allows the contribution of all the immune complexes present in the trap to be measured. Moreover, the porous nature of the microparticles packing through which the enzymatic substrate flows makes its interaction with the captured enzymes very efficient. This, together with the minimization of nonspecific interactions of proteins with the surfaces, leads to an excellent limit of detection.

The sensitivity achieved with our platform is among the highest reported using magnetic nanoparticles. There are articles documenting improved sensitivities using magnetic microparticles as immunosupport but with resulting test times in the order of hours whereby the total time required for our test is of 40 min.

The protocol described in this article was optimized for immunoassays with biotin as a model antigen. Although it might be necessary to optimize incubation times, flow rates, and perhaps surfaces functionalization for each particular case of immunoassays with different antigens and antibodies, the results obtained here with biotin show the excellent sensitivities that can be achieved with our device.

Apart from the flow of the substrate, another important flow in the operation of the device is the flow of the nanoparticles through the magnetic trap when they are being captured. This flow must be such that it saturates the magnetic nanoparticle trap in a reasonable time. The saturation of the trap depends on the flow rate, the concentration of nanoparticles, and the size of the magnetic trap (see Fig. S3 of the supplementary material).

In this work, we concentrated in exploring the limit of detection of our system, but we did not study its dynamic range, which depends on the flow rate (see Fig. 7). In fact, an important feature of our system is that its sensitivity strongly depends on the concentration ratio of the AbI and the nanoparticles: for a given concentration of AbI, the lower the concentration of nanoparticles, the larger the detection signal, although it will also take more time for the trap to saturate.[7] However, if the concentration of AbI becomes too large, at some point, it is expected that the signal from the trap will be no longer sensitive to concentration changes. But if that is the case, it suffices to increase the concentration of nanoparticles to recover the signal. The problem is that the concentration of AbI in a real sample is *a priori* unknown. In our case, we chose the concentration of nanoparticles optimized for the detection of low concentration of AbI, based on the work by Teste *et al.*[7] But in a real situation, where the concentration of AbI is unknown, our system would allow to perform several tests in parallel where different concentrations of nanoparticles would be used in each channel, thus extending the dynamic range of the system.

IV. CONCLUSIONS

We show the operation of a simple microfluidic device easily manufactured by micromilling of a low cost thermoplastic acrylic to perform sensitive and rapid immunoassays in continuous flow.

Short total assay times were obtained, thanks to the use of magnetic nanoparticles as immune support. They were able to accelerate the interactions between antigens and antibodies and reduce incubation times due to their colloidal properties.

For the separation and concentration of the nanoparticles, a porous magnetic trap composed of iron microparticles was used, which were covered with a layer of silica and PEG. The characterization analysis confirmed that the surface of the microparticles was homogeneously coated. It was found that the coating gives the microparticles resistance to oxidation and also reduces nonspecific interactions against nanoparticles and proteins.

Nonspecific interactions of proteins with the surface of the acrylic channels were also minimized with a novel one-step coating using a silane functionalized with PEG.

For the detection stage, antibodies labeled with the enzyme alkaline phosphatase were used, which lead to excellent sensitivity.

The combination of all these features, i.e., use of magnetic micro–nanoparticles, optimization of surfaces functionalization, and detection based on a fluorogenic enzyme, allowed our system to reach a detection limit of antibiotin antibody of 8 pg/ml in 40 min of assay time. The detection limit achieved with our device is among the highest reported using magnetic nanoparticles, with the added advantage of maintaining a short total assay time.

The reagents used for our immunoassay are all commercial and, therefore, the system can be easily adapted to use with other antigens and antibodies. However, the protocol, and probably also the functionalization of the surfaces, may be needed to be optimized for each specific use. Moreover, the system needs to be tested with clinically relevant antigens with high dissociation equilibrium constants and biological samples with an abundance of nontargets.

Real performance optimization requires additional studies, but this is the first step in the developing of a sensitive and rapid immunoassay with outstanding features.

All steps of the immunoassay were performed inside the device and, while supporting equipment was needed for the assay, the system can be easily compacted, automatized, and made independent of such equipment in order to develop point of care medical diagnostic devices: the microscope could be replaced by a low-cost miniaturized solution;[43] flow control of reagents could be done using microfluidic acrylic pumps and valves, which makes it compatible with low-cost mass production;[28] and the electromagnet can be replaced by a simple magnet for this application since the release of nanoparticles is not needed.[27] Moreover, we showed that tests can be performed in several traps in tandem, which opens up the possibility of designing a point of care device which could make a calibration curve for each test, in the same way in which a standard ELISA test works, while also providing quantitative results.

SUPPLEMENTARY MATERIAL

See the supplementary material for (1) a table with a revision of the literature about the use of micro- and nanoparticles in microfluidic systems for immunoassays, (2) the chip bonding protocol, (3) the XPS analysis of microparticles, (4) the nanoparticles trapping efficiency, (5) nonspecific interactions tests, (6) functioning of the three traps in parallel, and (7) the coated and uncoated microparticles' size distribution.

ACKNOWLEDGMENTS

This work has been supported by Conacyt, Mexico, under Grant Fronteras de la Ciencia No. 2015-2/1178. P.E.G.-P. thanks Conacyt for financial support. Analysis and assistance for SEM (Nayeli Pineda, CIMAV Monterrey), XPS (Luis Gerardo Silva, CIMAV Monterrey), TGA (Alberto Toxqui, CIMAV Monterrey), and particle size by Master Sizer (Lilia Bautista, CIMAV Monterrey) are thanked. We also thank Wendy Pérez Valdez for helping with the analytical techniques.

REFERENCES

[1]P. Yager, T. Edwards, E. Fu, K. Helton, K. Nelson, M. R. Tam, and B. H. Weigl, Nature **442**, 412 (2006).
[2]M. Urdea, L. A. Penny, S. S. Olmsted, M. Y. Giovanni, P. Kaspar, A. Shepherd, P. Wilson, C. A. Dahl, S. Buchsbaum, G. Moeller, and D. C. Hay Burgess, Nature **444**, 73 (2006).
[3]C. P. Price and L. J. Kricka, Clin. Chem. **53**, 1665 (2007).
[4]K. M. Koczula and A. Gallotta, Essays Biochem. **60**, 111 (2016).
[5]Q. Xu, H. Xu, H. Gu, J. Li, Y. Wang, and M. Wei, Mater. Sci. Eng. C **29**, 702 (2009). .
[6]S. Sharma, J. Zapatero-Rodríguez, P. Estrela, and R. O'Kennedy, Biosensors **5**, 577 (2015).
[7]B. Teste, F. Malloggi, J.-M. Siaugue, A. Varenne, F. Kanoufi, and S. Descroix, Lab Chip **11**, 4207 (2011).
[8]N. Pamme, Lab Chip **6**, 24 (2006).
[9]F. Lacharme, C. Vandevyver, and M. A. M. Gijs, Anal. Chem. **80**, 2905 (2008).
[10]B. Teste, F. Kanoufi, S. Descroix, P. Poncet, T. Georgelin, J.-M. Siaugue, J. Petr, A. Varenne, and M.-C. Hennion, Anal. Bioanal. Chem. **400**, 3395 (2011).
[11]B. Teste, F. Malloggi, A.-L. Gassner, T. Georgelin, J.-M. Siaugue, A. Varenne, H. Girault, and S. Descroix, Lab Chip **11**, 833 (2011).
[12]D. Witters, K. Knez, F. Ceyssens, R. Puers, and J. Lammertyn, Lab Chip **13**, 2047 (2013).
[13]Z. Huang, N. A. Olson, W. You, and R. P. Haugland, J. Immunol. Methods **149**, 261 (1992).
[14]J. P. Gosling, "Enzyme immunoassay," *Immunoassay* (Academic Press, San Diego, 1996), pp. 287–308.
[15]J. R. Trantum, D. W. Wright, and F. R. Haselton, Langmuir **28**, 2187 (2012).
[16]L. A. Sasso, A. Ündar, and J. D. Zahn, Microfluid. Nanofluidics **9**, 253 (2010).
[17]D. Tang, Y. Yu, R. Niessner, M. Miró, and D. Knopp, Analyst **135**, 2661 (2010).
[18]M. L. Frisk, G. Lin, E. A. Johnson, and D. J. Beebe, Biosens. Bioelectron. **26**, 1929 (2011).
[19]M. Herrmann, E. Roy, T. Veres, and M. Tabrizian, Lab Chip **7**, 1546 (2007).
[20]J.-U. Shim, R. T. Ranasinghe, C. A. Smith, S. M. Ibrahim, F. Hollfelder, W. T. S. Huck, D. Klenerman, and C. Abell, ACS Nano **7**, 5955 (2013).
[21]Y. H. Tennico, D. Hutanu, M. T. Koesdjojo, C. M. Bartel, and V. T. Remcho, Anal. Chem. **82**, 5591 (2010).
[22]L. Song, D. W. Hanlon, L. Chang, G. K. Provuncher, C. W. Kan, T. G. Campbell, D. R. Fournier, E. P. Ferrell, A. J. Rivnak, B. A. Pink, K. A. Minnehan, P. P. Patel, D. H. Wilson, M. A. Till, W. A. Faubion, and D. C. Duffy, J. Immunol. Methods **372**, 177 (2011).
[23]D. M. Rissin, C. W. Kan, T. G. Campbell, S. C. Howes, D. R. Fournier, L. Song, T. Piech, P. P. Patel, L. Chang, A. J. Rivnak, E. P. Ferrell, J. D. Randall, G. K. Provuncher, D. R. Walt, and D. C. Duffy, Nat. Biotechnol. **28**, 595 EP (2010).
[24]C. W. Kan, A. J. Rivnak, T. G. Campbell, T. Piech, D. M. Rissin, M. Mösl, A. Peterça, H.-P. Niederberger, K. A. Minnehan, P. P. Patel, E. P. Ferrell, R. E. Meyer, L. Chang, D. H. Wilson, D. R. Fournier, and D. C. Duffy, Lab Chip **12**, 977 (2012).
[25]L. Chang, L. Song, D. R. Fournier, C. W. Kan, P. P. Patel, E. P. Ferrell, B. A. Pink, K. A. Minnehan, D. W. Hanlon, D. C. Duffy, and D. H. Wilson, J. Virol. Methods **188**, 153 (2013).
[26]M. Herrmann, T. Veres, and M. Tabrizian, Lab Chip **6**, 555 (2006).
[27]P. E. Guevara-Pantoja and G. A. Caballero-Robledo, RSC Adv. **5**, 24635 (2015).
[28]P. E. Guevara-Pantoja, R. J. Jiménez-Valdés, J. L. García-Cordero, and G. A. Caballero-Robledo, Lab Chip **18**, 662 (2018).
[29]P. E. Guevara-Pantoja, O. Chávez-Pineda, A. M. Solis-Serrano, J. L. García-Cordero, and G. A. Caballero-Robledo, "An affordable 3D-printed positioner improves the Z resolution of conventional micromilling machines for microfluidics applications" (unpublished).
[30]J. Jiang, J. Zhan, W. Yue, M. Yang, C. Yi, and C.-W. Li, RSC Adv. **5**, 36036 (2015).
[31]S. Jo and K. Park, Biomaterials **21**, 605 (2000).
[32]Y. Lu, Y. Yin, B. T. Mayers, and Y. Xia, Nano Lett. **2**, 183 (2002).
[33]W. Stöber, A. Fink, and E. Bohn, J. Colloid Interface Sci. **26**, 62 (1968).
[34]T. Serizawa, S. Kamimura, N. Kawanishi, and M. Akashi, Langmuir **18**, 8381 (2002).
[35]C. C. Dupont-Gillain and P. G. Rouxhet, Nano Lett. **1**, 245 (2001).
[36]J. Liu, T. Pan, A. T. Woolley, and M. L. Lee, Anal. Chem. **76**, 6948 (2004).
[37]Y. Xie, C. A. Hill, Z. Xiao, H. Militz, and C. Mai, Compos. A Appl. Sci. Manuf. **41**, 806 (2010).
[38]K. Kim, S. W. Park, and S. S. Yang, Biochip J. **4**, 148 (2010).
[39]X. Wen, H. He, and L. J. Lee, J. Immunol. Methods **350**, 97 (2009).
[40]X. Sun, J. Liu, and M. L. Lee, Electrophoresis **29**, 2760 (2008).
[41]M. Cvek, M. Mrlik, M. Ilcikova, T. Plachy, M. Sedlacik, J. Mosnacek, and V. Pavlinek, J. Mater. Chem. C **3**, 4646 (2015).
[42]D. J. Anderson, Clin. Chem. **35**, 2152 (1989).
[43]R. A. Mendoza-Gallegos, A. Rios, and J. L. Garcia-Cordero, Anal. Chem. **90**, 5563 (2018).